BUILD SIMUL
https://doi.org/10.1007/s12273-018-0479-z

A new mathematical model for multi-scale thermal management of data centers using entransy theory

Hao Tian[1], Hang Liang[2] (✉), Zhen Li[3]

1. Changchun Institute of Optics, Fine Mechanics and Physics, Chinese Academy of Sciences, Changchun 130033, China
2. Norman Bethune Health Science Center, Jilin University, Changchun130021, China
3. Key Laboratory of Thermal Science and Power Engineering of Ministry of Education, Department of Engineering Mechanics, Tsinghua University, Beijing 100084, China

Research Article

Indoor/Outdoor Airflow and Air Quality

Abstract

Based on entransy theory, this paper proposes a new mathematical model for multi-scale data center thermal management. A comparison of heat transfer optimizing is made first, using exergy/entropy method and entransy dissipation, to verify the fitness of entransy theory. Based on which, a complete model of entransy dissipation for data center heat transfer is built, from CPU level to data center room level, with detailed computational derivation. Specifically, the calculating method of entransy dissipated by undesired air mixing has been derived, which can give quantitative evaluation on air mixing to the entire thermal performance of data center. A case study of a CFD simulation and a CRAC retrofitting engineering have been performed to verify the entransy model. In the case study, the temperature penalty caused by undesired air mixing is calculated using the entransy analysis model and testified by the retrofitting test, which directly reduces the free cooling potential and decrease data center energy performance. This entransy theory based model offers a new method to better optimize the thermal management and gives specific measures to improve the thermal performance of data centers.

Keywords

entransy theory,
entransy dissipation model,
data center,
air mixing,
thermal management

Article History

Received: 7 April 2018
Revised: 8 September 2018
Accepted: 12 September 2018

1 Introduction

During the past decades, with the increasing demand for massive compute and storage, more and more data centers have been built or updated. As a result, the power consumed by data centers sharply increases. Single cabinet load increases from less than 1 kW in early 1990s to over 30 kW in 2016 (Fulpagare and Bhargav 2015). Meanwhile, due to the widely use of high performance chips, the heat flux of server motherboard rises to nearly 20 W/cm^2 (Zhang et al. 2014). Hot spot has become a fetal threat to thermal health and security for data centers (Ebrahimi et al. 2014; Garimella et al. 2013). According to recent statistics, more than 30% of operating cost is spent on air-conditioning, and this number is going to exceed 50% in next five years (Ham et al. 2015).

The objective of data center thermal management is to maintain IT facility temperature and power consumption within a reasonable range. So far, many models have been proposed to analyze the heat transfer performance and fluid behavior in data centers (Tian et al. 2015; Gao et al. 2015; Carbó et al. 2016; Nada et al. 2015a,b, 2016a,b,c; Nada and Elfeky 2016; Priyadumkol and Kittichaikarn 2014; Almoli et al. 2012). Many models use CFD simulation, which bases on Navier–Stokes equations for fluid flow coupled with continuity equation and heat transfer equation. However, CFD method is time-consuming, sensitive to grid number and mesh quality. Therefore, CFD model is rarely used to real-time simulation of full-scale data centers. Other researchers propose specialized index or parameter (Sharma et al. 2002; Herlin 2005; Shrivastava et al. 2009) to better assess, evaluate or predict the performance of data center thermal management.

Recent years, useful work has been done to deeply optimize CFD algorithm and solvers, and make CFD method more suitable for large-scale real-time simulations. Song (2016) created a 3D compact axial-flow fan model to simulate the

E-mail: lianghang13@mails.jlu.edu.cn

swirling flow without considering the details of fan blade. The swirling speed is calculated by empirical relationship. Zhou and Yang (2008, 2010) used multiple reference frame (MRF) method and RNG k–ε model to numerically compute a CPU fan curve, which has only 8% discrepancy with the experimental data.

For the integrated thermal management of large data centers, building the full-scale heat transfer model is expensive. Missirlis et al. (2005, 2007) used a porous medium model to simulate the hydraulic and thermal behavior of CRAC units. Kritikos et al. (2010) and Yakinthos et al. (2007) used the revised model to analyze heat transfer in staggered heat exchanger, with the discrepancy with tested data less than 5%.

With more experimental support, many research use simplified server model to optimize cabinet heat transfer performance. Choi et al. (2008) used a simplified server model to analyze the relation between server load and cabinet thermal performance. Van Gilder et al. (2013) created a compact server model and incorporate it into CFD solvers to perform a transient heat transfer simulation.

A detailed comparison has been performed between different models for data center thermal analysis and management (Rambo and Joshi 2007; Zhou et al. 2012). Among these models, He et al. (2016) proposed a new analysis method, using temperature rise distribution to evaluate the influence of hot air re-circulation on data center thermal performance. This method has been verified by engineering testing.

Effort has also been spent on improvement of data center thermodynamic performance. Exergy has been used to optimize data center thermal management, based on the availability of useful work (Amip 2005).

Essentially, exergy theory comes from the second law of thermodynamics and is suitable to optimize heat work conversion process. As to heat transfer optimization, is exergy still the optimal theory? Here is a case study to answer this question.

A heat transfer process is built and illustrated by Fig. 1. There are two heat exchangers labeled as HEX_1 and HEX_2. Heat transfer ability is UA_1 and UA_2 (kW/K). Two heat exchangers are connected to a distributor. With the assumption of infinite flow rate, the input/output fluid temperature is fixed at T_1 and T_2 (K). Hot fluid flows into the distributor with temperature T_{in} (K) and flow rate CM (kg/s). The distributor separates the input hot fluid into two fluids with individual flow rate of CM_1 and CM_2 (kg/s) respectively ($CM = CM_1 + CM_2$).

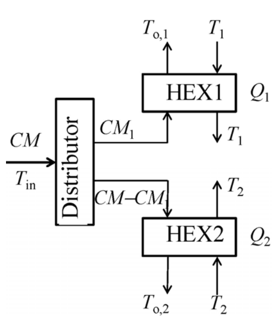

Fig. 1 Solo heat transfer process for verification

With the limitation of given UA ($UA = UA_1 + UA_2$), the object is to find the optimal UA_1 and UA_2 to maximize the total heat $Q = Q_1 + Q_2$.

The heat Q, exergy loss ΔE_x (reference temperature T_0=303 K) and entropy generation S_g can be calculated using follow formulas:

$$
\begin{aligned}
Q = Q_1 + Q_2 &= CM_1\left(T_{in} - T_1\right)\left(1 - e^{-\frac{UA_1}{CM_1}}\right) \\
&\quad + CM_2\left(T_{in} - T_2\right)\left(1 - e^{-\frac{UA_2}{CM_2}}\right)
\end{aligned}
$$

$$
\begin{aligned}
\Delta E_x &= \Delta E_{x,1} + \Delta E_{x,2} \\
&= CM_1\left(T_{in} - T_{o,1} - T_0 \ln\frac{T_{in}}{T_{o,1}}\right) - Q_1\left(1 - \frac{T_0}{T_1}\right) \\
&\quad + CM_2\left(T_{in} - T_{o,2} - T_0 \ln\frac{T_{in}}{T_{o,2}}\right) - Q_2\left(1 - \frac{T_0}{T_2}\right) \\
&= \left(Q_1\frac{T_0}{T} - CM_1 T_0 \ln\frac{T_{in}}{T_{in} - \frac{Q_1}{CM_1}}\right) \\
&\quad + \left(Q_2\frac{T_0}{T_2} - CM_2 T_0 \ln\frac{T_{in}}{T_{in} - \frac{Q_2}{CM_2}}\right)
\end{aligned}
$$

$$
\begin{aligned}
\dot{S}_g &= \dot{S}_{g,1} + \dot{S}_{g,2} = \left(CM_1 \ln\frac{T_{o,1}}{T_{in}} + \frac{Q_1}{T_1}\right) + \left(CM_2 \ln\frac{T_{o,2}}{T_{in}} + \frac{Q_2}{T_2}\right) \\
&= \left(CM_1 \ln\left(1 - \frac{Q_1}{T_{in}CM_1}\right) + \frac{Q_1}{T_1}\right) \\
&\quad + \left(CM_2 \ln\left(1 - \frac{Q_2}{T_{in}CM_2}\right) + \frac{Q_2}{T_2}\right)
\end{aligned}
$$

Figure 2 shows the variation of Q, ΔE_x and S_g with increment of UA_1.

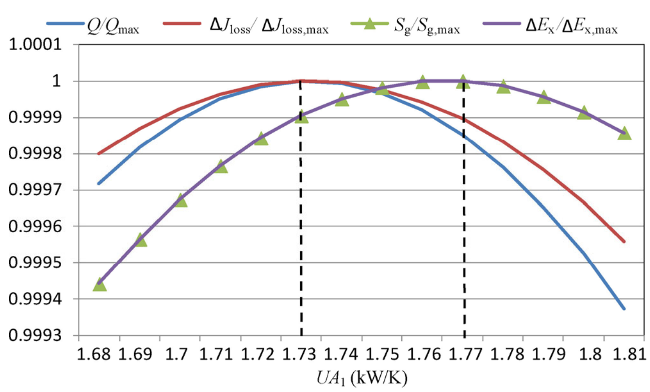

Fig. 2 Variation of transported heat, exergy loss, entropy generation and entransy dissipation with increment of heat transfer ability UA_1

Figure 2 tells that, with the increase of heat exchanger area UA_1, the optimal total heat Q corresponds to the optimal entransy loss ΔJ, not the optimal exergy loss ΔE_x or optimal entropy generation S_g. This indicates that entransy analysis better fits the optimization of heat transfer process.

2 Entransy dissipation model

Recent years, a new physical quantity called entransy to describe heat transfer potential, by analogy with electric field was proposed (Guo et al. 2003, 2007; Guo 2008; Cheng et al. 2011; Liu et al. 2011; Xu 2011). Deep analysis and argumentation on entransy theory has been started since then (Chen et al. 2013, 2015; Cheng and Liang 2018; Han et al. 2017; Hua et al. 2018; Goudarzi and Talebi 2018; Wang et al. 2018a,b,c; Wang and Zhu 2017; Wei et al. 2017, 2018; Wen et al.2018; Zhou et al. 2015). Principle of least entransy dissipation has been proposed and testified as a new guideline for heat transfer optimization (Guo et al. 2003; Wei et al. 2018). So far, entransy dissipation analysis has been used in analysis, comparison and optimal design of heat transfer related regions.

In electric filed, with the same potential difference, the more quantity of electricity a body carried, the more field work occurs, and more potential energy is lost. By analogy, in temperature field, the heat flux q driven by temperature difference δT always causes an irreversible dissipation. Such irreversible dissipation represents a potential energy loss, which can be quantified as $\Delta J = q \times \delta T$. ΔJ is defined as entransy dissipation, which represents the irreversible loss of heat transfer ability. The entransy J is a state quantity described by heat flux q and temperature T as $J = q \times T$. Thus, the entransy dissipation ΔJ during a heat transfer process from initial state (q_1,T_1) to final sate (q_2,T_2), can be computed as $\Delta J = q_1 \times T_1 - q_2 \times T_2$.

For a continuous heat transfer process in temperature field

$$\Delta J = \int_{T_1}^{T_2} q(T)\,\mathrm{d}T \tag{1}$$

Equation (1) provides a new graphical expression of entransy flow and dissipation in temperature-heat coordinate, called T–Q chart. Figure 3 is a T–Q chart for a steady state heat transfer process, with constant heat source/cold source temperature of T_h/T_c. The inlet/outlet temperature of hot fluid and cold fluid is represented by T_{in}/T_o and T_c/T_l respectively.

For the heat transfer process from heat source (T_h) to hot fluid (T_{in}/T_o), according to Eq. (1), the entransy dissipation ΔJ_h can be calculated as

$$\Delta J_h = \int_{T_{in}}^{T_o} (T_h - T)\,\mathrm{d}q = \int_{T_{in}}^{T_o} (T_h - T)(cm\,\mathrm{d}T) = cm(T_o - T_{in})\left[T_h - \frac{1}{2}(T_o + T_{in})\right] = q\Delta T_{mean} \tag{2}$$

In Eq. (2), cm represents heat capacity flow rate of the fluid (W/K); q stands for the heat (W); ΔT_{mean} refers to the mean temperature difference between heat source and hot fluid (K); ΔJ_h is graphically illustrated by the yellow region in T–Q chart of Fig. 3.

For heat transfer process between the two fluids, according to Eq. (1), the entransy dissipation ΔJ_l can be calculated as

$$\Delta J_l = \int_{T_{in}-T_c}^{T_o-T_l} \Delta T\,\mathrm{d}q = \int_{T_{in}-T_c}^{T_o-T_l} \Delta T\,\mathrm{d}(KF\Delta T) = \frac{1}{2}KF\left[(T_o - T_l)^2 - (T_{in} - T_c)^2\right] \tag{3}$$

The heat flux q can be written by the integral form:

$$q = \int \mathrm{d}q = \int_{T_{in}-T_c}^{T_o-T_l} KF\,d(\Delta T) = KF[(T_o - T_l) - (T_{in} - T_c)] \tag{4}$$

Bringing Eq. (4) back into Eq. (3), the entransy dissipation ΔJ_l can be written as

$$\Delta J_l = q\frac{1}{2}[(T_o - T_l) - (T_{in} - T_c)] = q\Delta T_{mean} \tag{5}$$

In Eqs. (3) to (5), KF represents heat transfer ability for each integral unit (W/K), and it is assumed to be constant during heat transfer process. ΔT is the temperature difference between two fluids for each integral unit (K). ΔJ_l is illustrated by the green region in T–Q chart of Fig. 3.

Using the same derivation as Eq. (2), the entransy dissipation ΔJ_c between the cold fluid and cold source can be written as

$$\Delta J_c = \int_{T_c}^{T_l} (T - T_c)(cm\,\mathrm{d}T) = cm\int_{T_c}^{T_l} T\,\mathrm{d}T - cmT_c\int_{T_c}^{T_l} \mathrm{d}T = cm(T_l - T_c)\left[\frac{1}{2}(T_l + T_c) - T_c\right] = \frac{1}{2}q(T_l - T_c) \tag{6}$$

ΔJ_c is illustrated by the blue region in T–Q chart of Fig. 3.

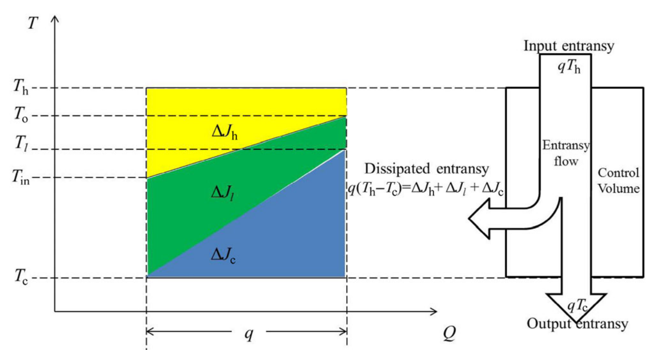

Fig. 3 T–Q chart of entransy flow and dissipation

The total entransy dissipation ΔJ during heat transfer process from hot source (T_h) to cold source (T_c) can be written as

$$\Delta J = \Delta J_h + \Delta J_l + \Delta J_c \tag{7}$$

Combining Eqs. (2), (5), (6) with Eq. (7) to calculate the total entransy dissipation ΔJ by Eq. (8):

$$\Delta J = q\left[T_h - \frac{1}{2}(T_o + T_{in})\right] + q\frac{1}{2}[(T_o - T_l) + (T_{in} - T_c)] + \frac{1}{2}q(T_l - T_c) = q(T_h - T_c) \tag{8}$$

With Eq. (8) and T–Q chart, entransy theory turns the analysis of a heat transfer network into a mathematical field model. All thermal behavior of heat transfer network can be expressed by entransy flow and entransy dissipation. Thus, a new mathematical solution for multi-scale thermal management of data centers becomes possible using the entransy model.

2.1 Entransy model of CPU level heat transfer process

The heat transfer process between CPU and cooling fluid (air, water, refrigerants, and so on) can be modeled as follows: a heat source with constant temperature T_{cpu}, and a fluid with inlet/outlet temperature of T_{in}/T_o, as illustrated by Fig. 4.

The CPU heat flux Q_{cpu} is assumed to be constant. According to Eq. (5), the entransy dissipation of CPU level heat transfer process can be calculated as

$$\Delta J_{cpu} = \frac{1}{2}Q_{cpu}[(T_{cpu} - T_{in}) + (T_{cpu} - T_o)] = Q_{cpu}\left[T_{cpu} - \frac{1}{2}(T_{in} + T_o)\right] \tag{9}$$

2.2 Entransy model of rack level heat transfer process

As to rack level heat transfer process, the undesired air mixing is a major problem, which is illustrated by Fig. 5. To quantify the effect of undesired air mixing, entransy model for air mixing process must be built.

For a steady state convective heat transfer process with constant fluid thermal properties and no internal heat source,

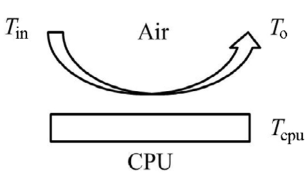

Fig. 4 CPU model with air cooling

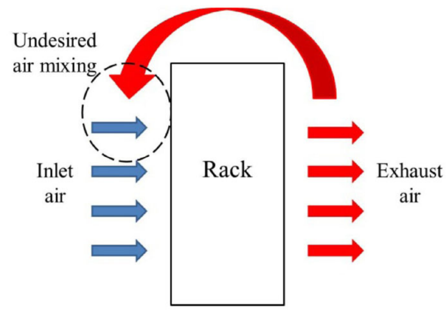

Fig. 5 Undesired air mixing in rack level

the energy balance equation is

$$\nabla \cdot (k\nabla T) = \rho c_p \vec{V} \cdot \nabla T \tag{10}$$

where, k represents fluid thermal conductivity (W/(m·K)); ρ represents fluid density (kg/m^3); c_p represents fluid specific heat (kJ/(kg·K)); $\vec{V}$ represents fluid velocity vector (m/s); T represents fluid thermal temperature (K).

Multiplying both sides of Eq. (10) by thermal temperature T to get Eq. (11):

$$T\nabla \cdot (k\nabla T) = \rho c_p T\vec{V} \cdot \nabla T \tag{11}$$

Performing vector deformation on the right side of Eq. (11) to get Eq. (12):

$$\rho c_p \vec{V}T \cdot \nabla T = \frac{1}{2}\rho c_p \vec{V} \cdot \nabla T^2 = \frac{1}{2}\rho c_p\left[\nabla \cdot \left(\vec{V}T^2\right) - T^2\nabla \cdot \vec{V}\right] \tag{12}$$

Putting mass conservation equation (continuity equation) $\nabla \cdot \vec{V} = 0$ into Eq. (12) to get Eq. (13):

$$\rho c_p \vec{V}T \cdot \nabla T = \nabla \cdot \left(\frac{1}{2}\rho c_p \vec{V}T^2\right) \tag{13}$$

Performing vector deformation on the left side of Eq. (11) to get Eq. (14):

$$T\nabla \cdot (k\nabla T) = \nabla \cdot (Tk\nabla T) - k(\nabla T)^2 \tag{14}$$

Putting Eq. (13) and Eq. (14) into Eq. (10) to get Eq. (15):

$$\nabla \cdot \left(\frac{1}{2}\rho c_p \vec{V}T^2\right) = \nabla \cdot (Tk\nabla T) - k(\nabla T)^2 \tag{15}$$

Defining convective entransy flow $\vec{J}_v$ (W·K/m^2) and conductive entransy flow $\vec{J}_t$ (W·K/m^2) as follows:

$$\vec{J}_v = \frac{1}{2}\rho c_p \vec{V}T^2 \tag{16}$$

$$\vec{J}_t = T\vec{q}_t = -Tk\nabla T \tag{17}$$

Putting Eq. (16) and Eq. (17) into Eq. (15) to get Eq. (18)

$$\nabla\cdot\vec{J}_{\mathrm{v}}+\nabla\cdot\vec{J}_{\mathrm{t}}=-k(\nabla T)^{2} \quad (18)$$

Terms on the left side of Eq. (18) $\nabla\cdot\vec{J}_{\mathrm{v}}$ and $\nabla\cdot\vec{J}_{\mathrm{t}}$ represent the variation of convective entransy flow $\vec{J}_{\mathrm{v}}$ and conductive entransy flow $\vec{J}_{\mathrm{t}}$ carried by the fluid, respectively. The term on right side of Eq. (18), $-k(\nabla T)^{2}$, represents heat transfer ability loss caused by irreversiblities. For a steady state convective heat transfer process with no internal heat source, Eq. (18) is the differential form of entransy conservation equation.

Integrating Eq. (18) in a control volume Ω, for a steady state convective heat transfer process in a finite volume, the integral form of entransy conservation equation is shown by Eq. (19):

$$\int_{\Omega}\left(\nabla\cdot\vec{J}_{\mathrm{v}}\right)\mathrm{d}\Omega+\int_{\Omega}\left(\nabla\cdot\vec{J}_{\mathrm{t}}\right)\mathrm{d}\Omega=\int_{\Omega}\left(-k(\nabla T)^{2}\right)\mathrm{d}\Omega \quad (19)$$

To convert the volume integral into surface integral, a deformation on the left terms of Eq. (19) is performed using Gauss Theorem, as shown by Eq. (20):

$$\oint_{S}\vec{J}_{\mathrm{v}}\cdot\mathrm{d}\vec{S}+\oint_{S}\vec{J}_{\mathrm{t}}\cdot\mathrm{d}\vec{S}=\oint_{S}\vec{J}_{\mathrm{v}}\cdot\vec{n}\mathrm{d}S+\oint_{S}\vec{J}_{\mathrm{t}}\cdot\vec{n}\mathrm{d}S$$
$$=\int_{\Omega}\left(-k(\nabla T)^{2}\right)\mathrm{d}\Omega \quad (20)$$

Equation (20) is the the differential form of entransy conservation equation for a steady state convective heat transfer process on the surface of a finite control volume Ω. $\vec{n}$ is the normal vector of the surface dS which surrounds the control volume Ω. For a cubic control volume illustated by Fig. 6, the normal vector of each surface is parallel to axis of Cartesian coordinates. In this case, Eq. (20) can be rewritten as Eq. (21):

$$\begin{aligned}&\frac{1}{2}\rho c_{\mathrm{p}}\Big[\left(V_{x,\mathrm{in}}\Delta Y\Delta ZT_{x,\mathrm{in}}^{2}+V_{y,\mathrm{in}}\Delta X\Delta ZT_{y,\mathrm{in}}^{2}+V_{z,\mathrm{in}}\Delta X\Delta YT_{z,\mathrm{in}}^{2}\right)\\&\quad-\left(V_{x,\mathrm{out}}\Delta Y\Delta ZT_{x,\mathrm{out}}^{2}+V_{y,\mathrm{out}}\Delta X\Delta ZT_{y,\mathrm{out}}^{2}+V_{z,\mathrm{out}}\Delta X\Delta YT_{z,\mathrm{out}}^{2}\right)\Big]\\&\quad-k\Big[\Big(T_{x,\mathrm{in}}\Delta Y\Delta Z\Big(\frac{\partial T}{\partial X}\Big)_{\mathrm{in}}+T_{y,\mathrm{in}}\Delta X\Delta Z\Big(\frac{\partial T}{\partial Y}\Big)_{\mathrm{in}}+T_{z,\mathrm{in}}\Delta X\Delta Y\Big(\frac{\partial T}{\partial Z}\Big)_{\mathrm{in}}\Big)\\&\quad-\Big(T_{x,\mathrm{out}}\Delta Y\Delta Z\Big(\frac{\partial T}{\partial X}\Big)_{\mathrm{out}}+T_{y,\mathrm{out}}\Delta X\Delta Z\Big(\frac{\partial T}{\partial Y}\Big)_{\mathrm{out}}+T_{z,\mathrm{out}}\Delta X\Delta Y\Big(\frac{\partial T}{\partial Z}\Big)_{\mathrm{out}}\Big)\Big]\\&=k\int_{\Omega}\Big(\Big(\frac{\partial T}{\partial X}\Big)^{2}+\Big(\frac{\partial T}{\partial Y}\Big)^{2}+\Big(\frac{\partial T}{\partial Z}\Big)^{2}\Big)\mathrm{d}\Omega\end{aligned} \quad (21)$$

For a cubic control volume illustrated by Fig. 7, the term, $\oint_{S}\vec{J}_{\mathrm{v}}\cdot\mathrm{d}\vec{S}/\oint_{S}\vec{J}_{\mathrm{t}}\cdot\mathrm{d}\vec{S}$, on the left side of Eq. (20) represent the net flux of convective entransy flow $\vec{J}_{\mathrm{v}}/\vec{J}_{\mathrm{t}}$ through the closed surface S, respectively. The term, $-k\int_{\Omega}(\nabla T)^{2}\mathrm{d}\Omega$, on the right side of Eq. (20) represents the net flux of all entransy flows through the closed surface S, which means the entransy dissipation of the convective heat transfer process within this control volume.

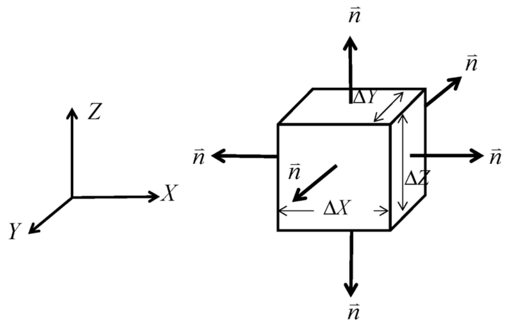

Fig. 6 Cubic control volume in data center space

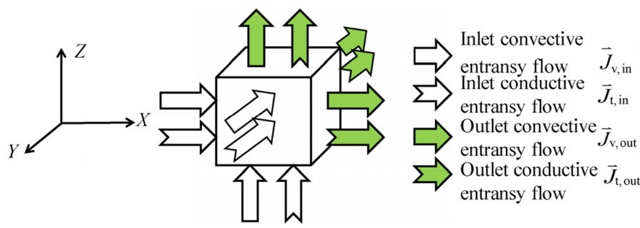

Fig. 7 Entransy flow into and out of space control volume

2.3 Entransy model of room level heat transfer

For a given data center with p CRAC units, n racks and m CPUs inside each rack, based on Eq. (7) to Eq. (8), the room level entransy dissipation model is shown by Eq. (22), in which J_{in} and J_{out} represent the input and output entransy flow, respectively.

$$\Delta J_{\mathrm{loss,room}}=J_{\mathrm{in}}-J_{\mathrm{out}}=\Delta J_{\mathrm{cpu}}+\Delta J_{\mathrm{mixing}}+\Delta J_{\mathrm{crac}} \quad (22)$$

The entransy flow J_{in} into the room is calculated by Eq. (23):

$$J_{\mathrm{in}}=\sum_{i=1}^{n\times m}Q_{\mathrm{cpu},i}T_{\mathrm{cpu},i} \quad (23)$$

The entransy flow J_{out} out of the room can be calculated Eq. (24):

$$J_{\mathrm{out}}=\sum_{j=1}^{p}Q_{\mathrm{crac},j}T_{\mathrm{crac},j} \quad (24)$$

The energy conservation equation is

$$\sum_{i=1}^{n\times m}Q_{\mathrm{cpu},i}=\sum_{j=1}^{p}Q_{\mathrm{crac},j} \quad (25)$$

A single rack can be modeled as a steady state open system with n CPUs and one inlet/outlet airflows. The temperature and mass flow rate for each inlet/outlet airflow is represented by $T_{\mathrm{a,in},i}/T_{\mathrm{a,o},i}$ and $CM_{\mathrm{a,in},i}/CM_{\mathrm{a,o},i}$, respectively. Assuming that air mixing takes place randamly among n CPUs. According to Eq. (20), the entransy dissipation $\Delta J_{\mathrm{mixing}}$ of rack level air mixing can be deduced as follows:

$$\Delta J_{\text{mixing}} = J_{\text{air,in,rack}} - J_{\text{air,out,rack}} = \sum_{i=1}^{n}\left(\frac{1}{2}CM_{\text{a,in},i}T_{\text{a,in},i}^{2} + Q_{\text{cpu},i}T_{\text{cpu},i} - \frac{1}{2}CM_{\text{a,o},i}T_{\text{a,o},i}^{2}\right) \tag{26}$$

CRAC unit can be modeled as a steady state open system with one refrigerant coil (cold source), one return air and one CRAC supply air. The temperature and mass flow rate for return/supply airflow is represented by $T_{\text{a,in},j}/T_{\text{a,o},j}$ and $CM_{\text{a,in},j}/CM_{\text{a,o},j}$, respectively. Refrigerant coil temperature is represented by $T_{\text{crac},j}$. Assuming that no air mixing occurs in CRAC units. According to Eq. (21), the entransy dissipation of CRAC heat exchange process ΔJ_{crac} can be deduced as follows:

$$\Delta J_{\text{crac}} = \sum_{j}\left(J_{\text{air,in,crac}} - J_{\text{air,out,crac}}\right) = \sum_{j=1}^{p}\left(\frac{1}{2}CM_{\text{a,in},j}T_{\text{a,in},j}^{2} - Q_{\text{crac},j}T_{\text{crac},j} - \frac{1}{2}CM_{\text{a,o},j}T_{\text{a,o},j}^{2}\right) \tag{27}$$

Bringing Eqs. (23) to (27) back into Eq. (22), the entransy dissipation model of a given data center room can be rewritten as follows:

$$\begin{aligned}\Delta J_{\text{loss,room}} &= \sum_{i=1}^{n\times m}Q_{\text{cpu},i}T_{\text{cpu},i} - \sum_{j=1}^{p}Q_{\text{crac},j}T_{\text{crac},j} - \sum_{i=1}^{n}\left(\frac{1}{2}CM_{\text{a,in},i}T_{\text{a,in},i}^{2} + Q_{\text{cpu},i}T_{\text{cpu},i}\right.\\ &\quad\left. - \frac{1}{2}CM_{\text{a,o},i}T_{\text{a,o},i}^{2}\right) - \sum_{j=1}^{p}\left(\frac{1}{2}CM_{\text{a,in},j}T_{\text{a,in},j}^{2} - Q_{\text{crac},j}T_{\text{crac},j} - \frac{1}{2}CM_{\text{a,o},j}T_{\text{a,o},j}^{2}\right)\\ &= \sum_{i=1}^{n}\left(\frac{1}{2}CM_{\text{a,in},i}T_{\text{a,in},i}^{2} - \frac{1}{2}CM_{\text{a,o},i}T_{\text{a,o},i}^{2}\right) + \sum_{j=1}^{p}\left(\frac{1}{2}CM_{\text{a,in},j}T_{\text{a,in},j}^{2} - \frac{1}{2}CM_{\text{a,o},j}T_{\text{a,o},j}^{2}\right)\\ &= \left(\sum_{i=1}^{n}\frac{1}{2}CM_{\text{a,in},i}T_{\text{a,in},i}^{2} + \sum_{j=1}^{p}\frac{1}{2}CM_{\text{a,in},j}T_{\text{a,in},j}^{2}\right) - \left(\sum_{i=1}^{n}\frac{1}{2}CM_{\text{a,o},i}T_{\text{a,o},i}^{2}\right.\\ &\quad\left. + \sum_{j=1}^{p}\frac{1}{2}CM_{\text{a,o},j}T_{\text{a,o},j}^{2}\right)\\ &= J_{\text{a,input}} - J_{\text{a,output}}\end{aligned} \tag{28}$$

Equation (28) indicates that, for a given data center room with adiabatic envelops, entransy dissipation of air mixing has nothing to do with servers or CRAC units.It is essentially determined by airflow characteristics.

Entransy dissipation of data center heat transfer process is illustrated by T–Q chart in Fig. 8. It is a universal model of entransy dissipation analysis for data center thermal management.

3 Case study

3.1 CFD simulation

For the data center model illustrated by Fig. 9. The room size is 8 m × 6 m × 3.6 m. Cooling air (blue arrow) is delivered from CRAC unit (1.2 m × 0.8 m × 1.8 m) to the pressurized

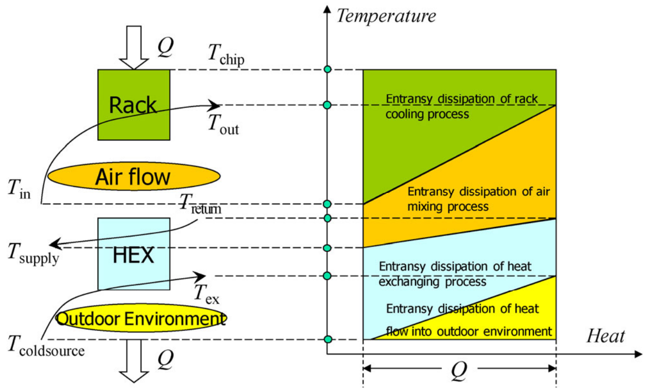

Fig. 8 Entransy dissipation of a typical data center heat transport path

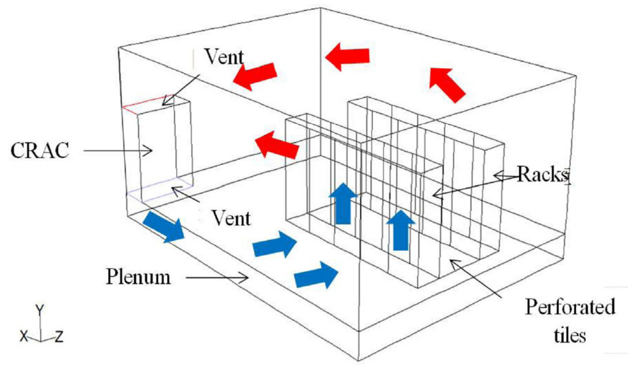

Fig. 9 Model of under-floor air distributed data center (ten racks with one CRAC unit)

under-floor plenum (height of 0.5 m). Cooling air is pushed into room space through the perforated tiles (each tile size of 0.8 m × 0.6 m , with open area ratio of 40%) at the raised floor. Cooling air is inhaled into racks (size of 1.8 m × 0.6 m × 0.6 m). The exhaust hot air (red arrow) is sent back to CRAC unit vent (size of 0.8 m × 0.5 m) through the upper space of the room. Two lines of racks form one cold asile and two hot aisles,with five racks in each line. Ten perforated tiles form the cold aisle area (size of 8.8 m × 1.2 m).

Based on the entransy dissipation model built above, an integrated CFD simulation of data center heat transfer and airflow is performed. The solver uses the commercial CFD software FLUENT. Considering large size of CRAC vents (0.8 m) and high speed airflow (2.5–3.5 m/s), the local flow pattern can be turbulence with high Reynolds number (10^5 order). Therefore, the standard k-ε model is used with standard wall function. The SIMPLEC algorithm is adopted to resolve the couple of pressure-velocity in fluid field. A second-order upwind solution is used for the accurate computation of momentum item. As for the energy item, the QUICK decrease scheme is used. The flow resistance type is Perforated Thin Vent.

Entransy flow and entransy dissipation equations are defiend using UDS and UDF. Viscous heating is not considered. TKE Prandtl Number is 1, TDR Prandtl Number is 1.3, Energy Prandtl Number is 0.85, Wall Prandtl Number is 0.85. Cmu value is 0.09, C1-Epsilon value is 1.44, C2-Epsilon is 1.92.

All other parameters use the default values of standard k-ε model in FLUENT software.

Grid independence validation has been performed to validate the data center model.

Walls of this data center model are set to be adiabatic, and all heat is removed by the CRAC unit. Cooling airflow rate inhaled by each rack is set to be 2000 m³/h. The total heat of all racks is set to be 60 kW. The supply cooling air temperature is set to be 293 K (20 °C), and the rated airflow rate of CRAC unit is set to be 20000 m³/h.

3.2 Result analysis

Entransy dissipation of air mixing in this data center model is calculated for each grid cell, using Eq. (29):

$$\Delta J_{\text{loss}} = \int_{\Omega}\left(k(\nabla T)^2\right)\mathrm{d}\Omega = k\int_{\Omega}\left(\left(\frac{\partial T}{\partial X}\right)^2+\left(\frac{\partial T}{\partial Y}\right)^2+\left(\frac{\partial T}{\partial Z}\right)^2\right)\mathrm{d}\Omega \tag{29}$$

Table 1 lists the heat, airflow rate and intake/exhaust air temperature for each rack in this model.

3.2.1 *Entransy dissipation fields*

The air temperature field and corresponding entransy dissipation field of data center room is illustrated by Fig. 10 to Fig. 17.

The simulation results show some useful information. Figure 12 shows that the largest temperature gradient locates at the hot aisle, with biggest temperature difference of 14 K. According to temperature field, hot aisles is considered as potential hot spots. And cold aisles are relatively safe, due to the low intake air temperature (293–301 K) and small temperature gradient (7–8 K). However, Fig. 13 tells that more attention should be paid to other regions, such as area near the bottom of cold aisles , area around the raised floor in hot aisles, and area around the top of racks. These regions do not be noticed from temperature field in Fig. 12, but are identified by entransy dissipation field. Entransy dissipation field tells where the work should be done to prevent the unnecessary air mixings. For example, setting local division plates to change the airflow path, guiding more hot air to flow directly to CRAC units. Entransy dissipation field tells thermal managers to put useful work and valuable resources to the right place.

Table 1 Numerical simulation results

Racks	Heat (kW)	Airflow rate (m³/h)	Inlet air temp (K)	Outlet air temp (K)
Rack 1	6.7	2000	300	310
Rack 2	8.7	2000	296	309
Rack 3	5.3	2000	295	303
Rack 4	6.0	2000	294	303
Rack 5	9.3	2000	294	308
Rack 6	4.0	2000	294	300
Rack 7	3.3	2000	294	299
Rack 8	10.7	2000	293	309
Rack 9	4.7	2000	293	300
Rack 10	7.3	2000	300	311
CRAC unit	66	20000	302.9	293

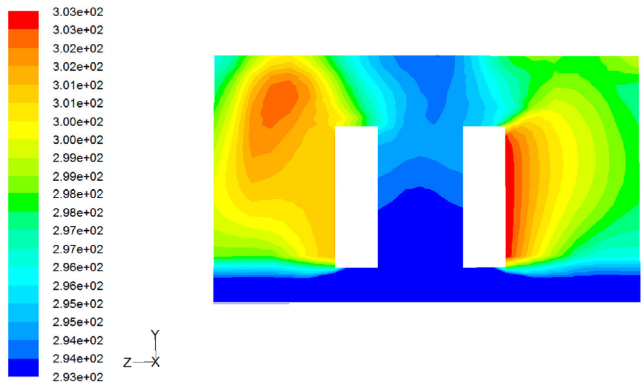

Fig. 10 Air temperature field (K) at $X = -2$ m cross section

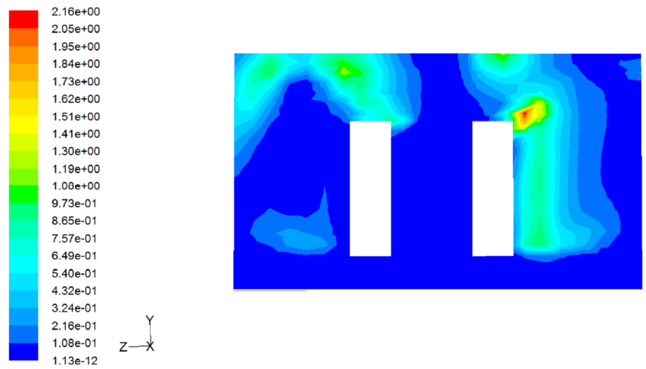

Fig. 11 Air mixing entransy dissipation (W·K) at $X = -2$ m cross section

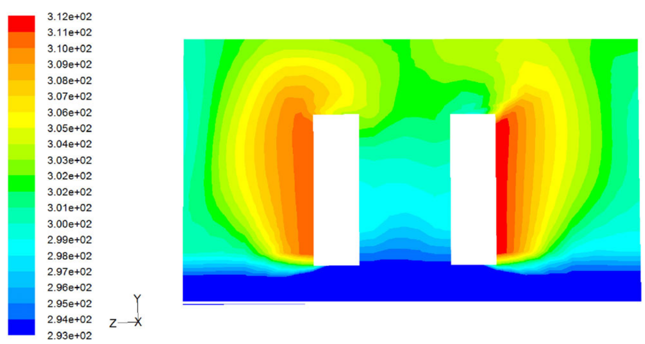

Fig. 12 Air temperature field (K) at $X = 0$ m cross section

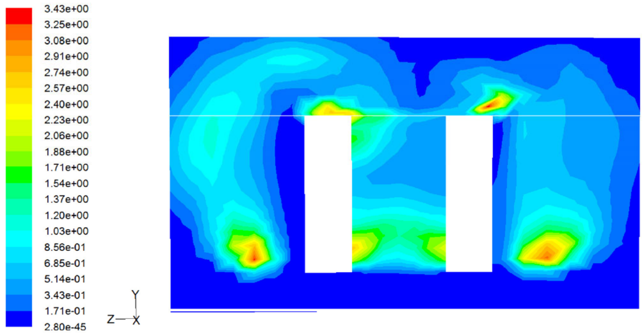

Fig. 13 Air mixing entransy dissipation (W·K) at X = 0 m cross section

Figure 15 shows that, entransy dissiaption of air mixing is non-uniform. By contrast, the temperature gradient of 13–14 K illustrated by Fig. 14 is uniformly distributed. This non-uniformity of entransy dissipation field can accurately tell where major heat transfer potential is lost, and where the measures must be taken.

Figure 17 indicates a significant entransy dissipation around CRAC vent. Such harmful air mixing close to CRAC vent will directly lower the return air temperature and chilled water temperature. Figure 17 gives more specific information where the measures of reducing air mixings will be most effective.

To sum up, compared to temperature field, the entransy dissipation field can precisely identify where the measure to prevent harmful air mixings will be most effective. Entransy dissipation field helps the thermal managers to adopt appropriate measures on the right place, and better improve data center thermal performance.

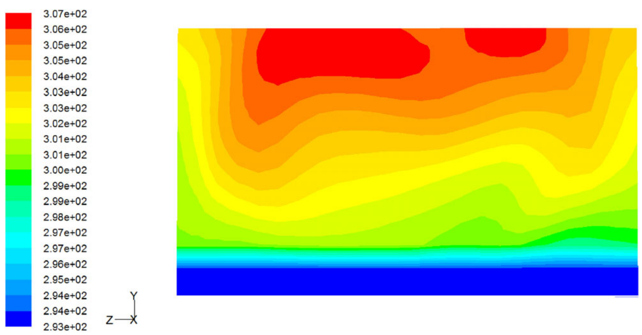

Fig. 14 Air temperature field (K) at X = 2 m cross section

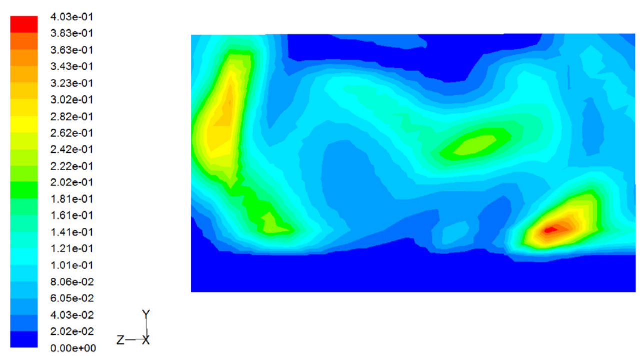

Fig. 15 Air mixing entransy dissipation (W·K) at X = 2 m cross section

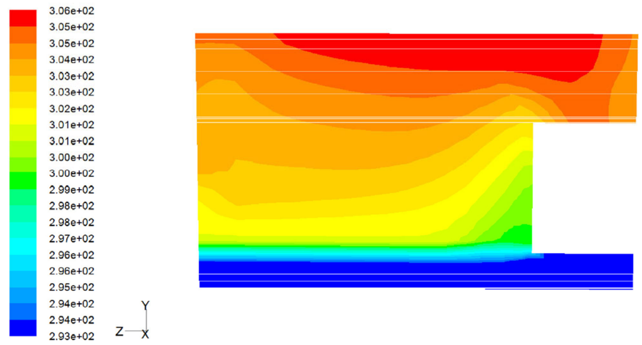

Fig. 16 Air temperature field (K) at X = 4 m cross section

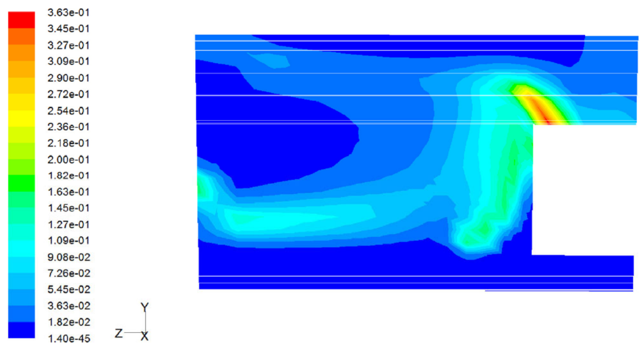

Fig. 17 Air mixing entransy dissipation (W·K) at X = 4 m cross section

3.2.2 *Free cooling potential*

According to Eq. (28) and Table 1, the total entransy dissipation of undesired air mixing in this data center model is calculated to be 196.3 kW·K. And this value will be 198.2 kW·K using cell integration method of Eq. (29). Considering the total heat of 60 kW, the temperature deviation computed by these two methods is 0.03 K (see Eq. (30) below). Such 0.03 K temperature deviation for cold source (e.g., chilled water or refrigerant) can be accepted.

$$\mathrm{d}T = \frac{\mathrm{d}J_{\text{mixing}}}{Q} = \frac{\mathrm{d}J_{\text{mixing}}}{\sum_{i=1}^{n} Q_{\text{rack},i}} = \frac{198.2 - 196.3}{60} = 0.03\ \text{K} \tag{30}$$

Dividing the total entransy dissipaton ΔJ_{loss} by total heat $Q = \sum_{i=1}^{n} Q_{\text{rack},i}$, the temperature cost ΔT paid for the entransy dissipation is as follows:

$$\Delta T = \frac{\Delta J_{\text{mixing}}}{Q} = \frac{\Delta J_{\text{mixing}}}{\sum_{i=1}^{n} Q_{\text{rack},i}} = \frac{196.3}{60} = 3.27\ \text{K} \tag{31}$$

Equation (31) shows that, the undesired air mixing costs additional 3.27 K to make up for the heat transfer ability loss. The cold source temperature has been forced to decrease by 3.27 K to finish the heat transfer process.

To quantify such 3.27 K cost on data center energy performance, Table 2 shows the statistical annual hours of outdoor wet bulb temperature for several typical cities in China. In this case, the maximum available wet bulb temperature is set to be 22 °C. This free cooling availability has to be decreased to 18.73 °C when the 3.27 K cost is considered.

With 3.27 K decrease, the four cities averagely reduces1000 hours of annual free cooling time. This means 10%–16% of free cooling potntial is wasted by air mixing.

3.3 Data center retrofitting

Based on the entransy dissipation analysis above, a fundamental solution to improve data center thermal management is to eliminate air mixing. With zero entransy dissipation of air mixing, higher temperature cold source with more free cooling potential can be expected.

To further represent the case analysis above, and give appropriate measures and specific methods of how entransy theory better improves thermal management of data centers, a more convincible case study of CRAC retrofitting is presented.

3.3.1 *Testing of thermal performance before retrofitting*

An operating data center of SINOPEC in Jilin (a city in northeast of China) is retrofitted. The basic information of this data center is listed in Table 3.

Figure 18 is the photo of the data center before retrofitting. The configuration of cold/hot aisles with raised floor plenum is used to physically separate hot air from cooling air. Cooling air is delivered from CRAC units to the pressurized underfloor plenum, then is pushed into data center room through the perforated tiles at the raised floor (called cold aisle). Cooling air is finally inhaled into racks which stand along the cold aisle. The hot exhaust air runs into a separated space between racks (called hot aisle) and finally returns to CRAC units.

Table 2 Statistical annual hours of outdoor air wet bulb temperature for several typical cities in China

City	Hours of $T_{wet} < 22$ °C	Hours of $T_{wet} < 18.73$ °C	Reduced hours	Percentage (%)
Harbin	8227	7279	948	11.5
Changchun	8620	7799	821	9.5
Beijing	7640	6533	1107	14.5
Shanghai	6669	5601	1068	16.0

Table 3 Basic information of the retrofitting case study data center in Jilin, China (before retrofitting)

Room size	36 m × 12 m × 3.6 m
Airflow organization	Cold/hot aisles with under-floor static box and perforated tiles
Rack number	65
Workload of a single rack	1628 kW
CRAC units number	9
Rated cooling capacity of a single CRAC unit	190 kW
Indoor temperature	19–28 °C
Indoor humidity	37%–65%

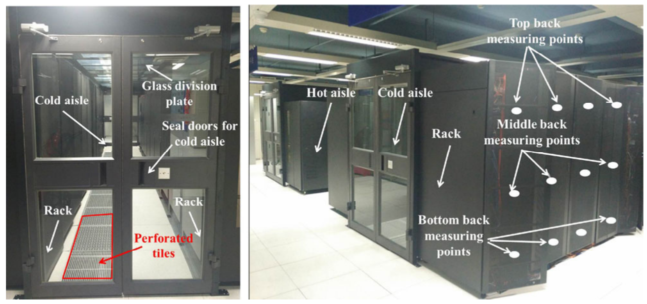

Fig. 18 Photo of Jilin SINOPEC data center before retrofitting in 2016

To further reduce the chance of air mixing between cold and hot aisles as much as possible, each aisle has been sealed by glass division plates at the top and two ends of each aisle.

The cold source is the combination of centrifuge water chillers and cooling towers. Free cooling is activated when the output water of cooling tower is cool enough.

For the state of the art, such design is almost perfect. However, the testing results show another way.

Figure 19(a) tests the hourly averaged supply air temperature of all 9 CRAC units, from 8:00 am to 6:00 pm on August 6th, 2016. The air temperature range is 18.2 °C to 20.6 °C, with maximum difference of 2.4 °C. Figure 19(b) tests the real time temperature of chilled water to CRAC units, during the same period. Chilled water temperature shows a tiny variation from 11.6 °C to 12.5 °C.

By contrast, Fig. 20 tests the hourly averaged intake and exhaust air temperature of 17 racks. from 8:00 am to 6:00 pm on August 6th, 2016. These 17 racks are contained by a sealed cold/hot aisle configuration.

Each rack has three measuring points along the front door, labeled as "bottom front", "middle front" and "top front". Correspondingly, three measuring points along the back door of each rack are labeled as "bottom back", "middle back" and "top back". The maximum temperature difference of intake air is 8.7 °C, and maximum temperature difference of exhaust air is 13.1 °C.

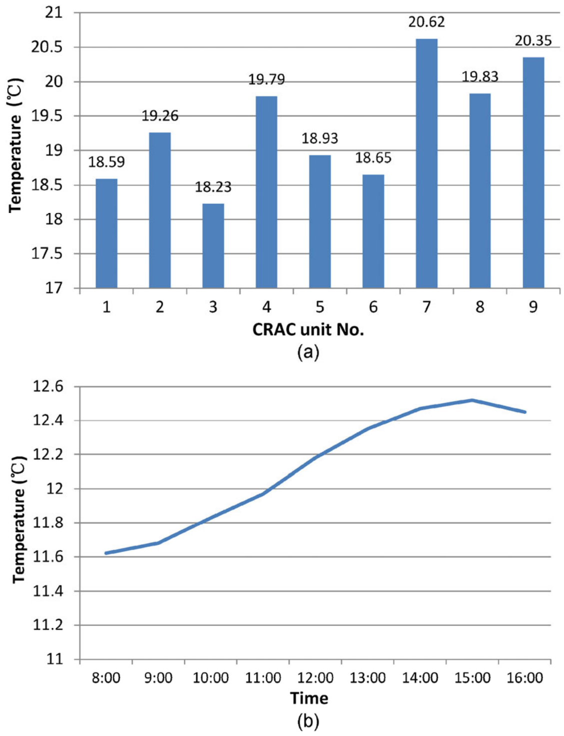

Fig. 19 (a) Hourly averaged supply air temperature of 9 CRAC units and (b) real time temperature of chilled water to CRAC units before retrofitting in 2016

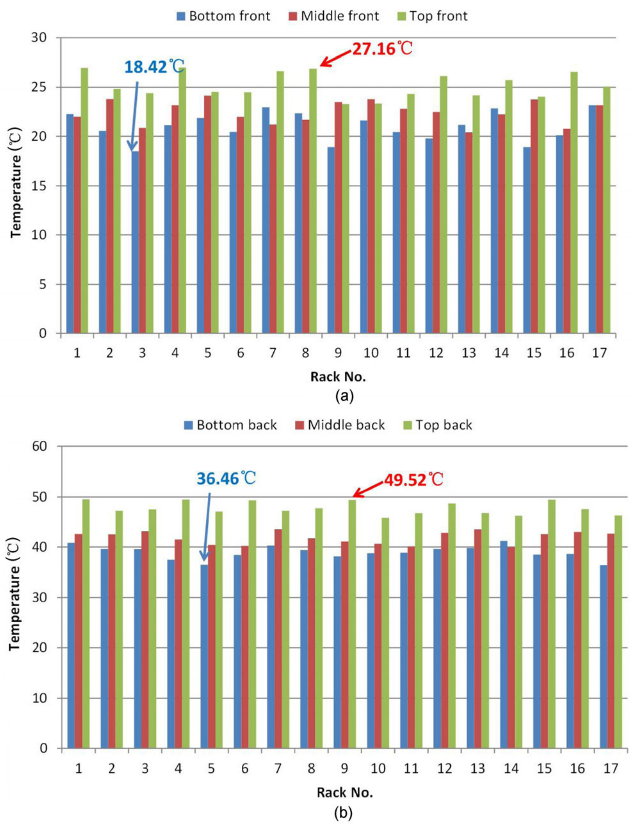

Fig. 20 (a) Hourly averaged intake air temperature of 17 racks and (b) hourly averaged exhaust air temperature of 17 racks before retrofitting in 2016

According to Eq. (28), the air mixing entransy dissipation of these 17 racks is calculated as 2210 kW·K. The corresponding temperature decrease of outdoor cold source is calculated as

$$\Delta T=\frac{\Delta J_{\text{mixing}}}{Q}=\frac{\Delta J_{\text{mixing}}}{\sum_{i=1}^{n=17} Q_{\text{rack},i}}=\frac{2210\ \text{kW}\cdot\text{K}}{425\ \text{kW}}=5.2\ \text{K} \tag{32}$$

It must be noticed that, entansy analysis is the only possible approach to get this 5.2 K of temperature cost. Traditional analysis using temperature field (e.g., Fig. 19 and Fig. 20) can not do this. This will be validated later by the retrofitting test.

Figure 21 labels the hot spots along the testing cold aisle. These hot spots indicate that, separated aisles and glass divisions do not eliminate air mixings. Physical methods alone do not work.

3.3.2 Cabinet cooling with inner heat pipe loops

To eliminate air mixing, a feasible solution is to shorten the air transport path as much as possible. Based on this principle, a cabinet cooling solution is proposed.

For a given cabinet of 1 kW, Fig. 22 and Fig. 23 illustrate two kinds of non-air-mixing cooling solutions, respectively. Figure 24 compares these two solutions using *T*–*Q* chart. The entransy analysis on these two solutions are performed and listed by Table 4 and Tabel 5.

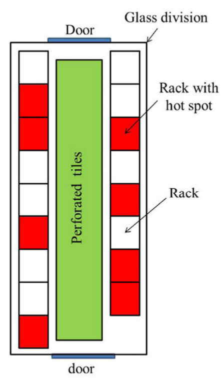

Fig. 21 Distribution of hot spots among the tested 17 racks

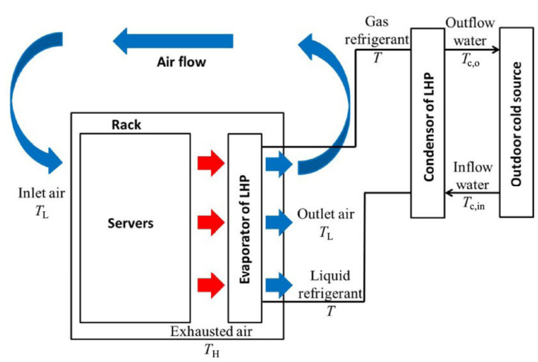

Fig. 22 Rack cooling with single-stage heat pipe loop

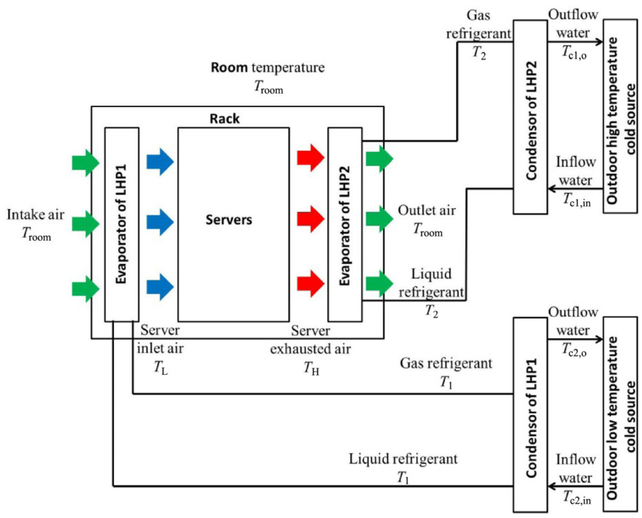

Fig. 23 Rack cooling with multi-stage heat pipe loop

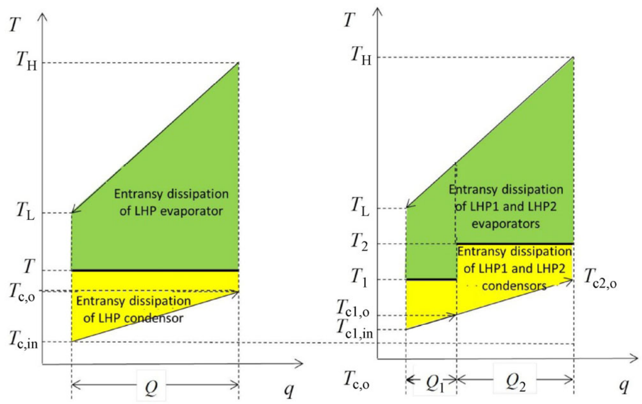

Fig. 24 Entransy dissipation comparison in T–Q chart

It can be seen that, compared with the solution of single-stage heat piple loop (15.50 kW·K), the multi-stage configuration has a lower entransy dissipation (12.92 kW·K). This means a temperature rise of 2.58 K for chilled water is earned. Such difference can also be seen from the green region in Fig. 24.

Considering the initial and operating cost, the final cooling solution uses two-stage heat pipe loops, as illustrated by Fig. 23. The first stage of heat pipe loop (LHP1) cools intake air from room temperature (24–26 °C) to 18–21 °C. The second stage of heat pipe loop (LHP2) cools server exhaust air from about 45 °C to room temperature (24–26 °C) again. Cooling capacity for each heat pipe loop is independently regulated by fans (see Fig. 25), based on server workload change. By this way, temperature difference between cabinet intake/exhaust air and indoor air is eliminated.

Cabinet cooling scheme is shown by Fig. 25. It cancels cold/hot aisles, CRAC units and raised floor plenum. Therefore, more room can be utilized to accommodate more cabinets.

The outdoor cold source (chillers and cooling towers) is not retrofitted.

The retrofitting is finished in 2017.

3.3.3 Test of thermal performance after retrofitting

A comparable testing is performed to verify entransy theory.

Figure 26 shows the hourly averaged temperature of intake and exhaust air for LHP1 and LHP2, respectively. Each temperature data uses the arithmetic average value of three measuring points. To guarantee the comparability,

Table 4 Performance of single-stage rack cooling (counter flow)

Rack inlet air temperature T_L	18 °C	Total heat transfer Q	1 kW
Rack exhausted air temperature T_H	36 °C	Entransy dissipation of LHP evaporator	11 kW·K
Media temperature of LHP T	16 °C	Entransy dissipation of LHP condenser	4.5 kW·K
Cooling fluid inlet temperature $T_{c,in}$	8 °C	Total entransy dissipation of LHP	15.5 kW·K
Cooling fluid outlet temperature $T_{c,o}$	15 °C		

Table 5 Performance of multi-stage rack cooling (counter flow)

Rack inlet air temperature T_L	18 °C	*NTU*1/*NTU*2	1
Rack exhausted air temperature T_H	36 °C	Heat transfer of LHP1 Q_1	0.39 kW
Media temperature of LHP1 T_1	14.8 °C	Heat transfer of LHP2 Q_2	0.61 kW
Cooling fluid inlet temperature $T_{c1,in}$	10.6 °C	Entransy dissipation of LHP1 evaporator	2.58 kW·K
Cooling fluid outlet temperature $T_{c1,o}$	13.3 °C	Entransy dissipation of LHP1 condenser	1.10 kW·K
Media temperature of LHP2 T_2	19.9 °C	Entransy dissipation of LHP2 evaporator	6.51 kW·K
Cooling fluid inlet temperature $T_{c2,in}$	13.3 °C	Entransy dissipation of LHP2 condenser	2.73 kW·K
Cooling fluid outlet temperature $T_{c2,o}$	17.6 °C	Total entransy dissipation of LHP1	3.68 kW·K
Room temperature T_o	25 °C	Total entransy dissipation of LHP2	9.24 kW·K
		Total entransy dissipation of LHP	12.92 kW·K

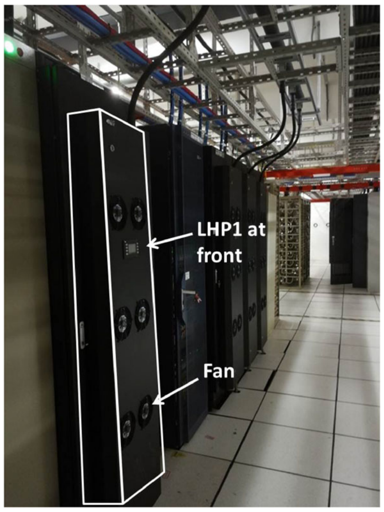

Fig. 25 Photo of new inner-cooled racks after retrofitting in 2017

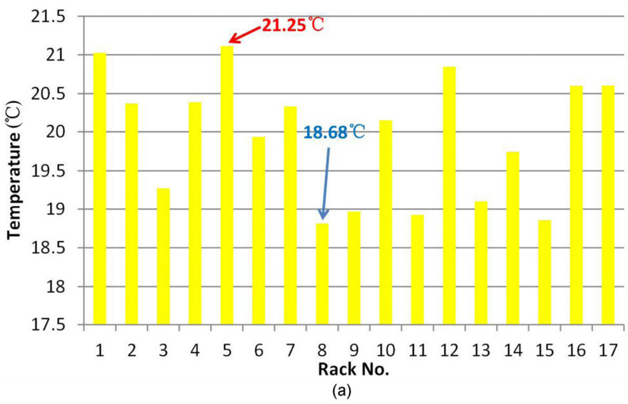

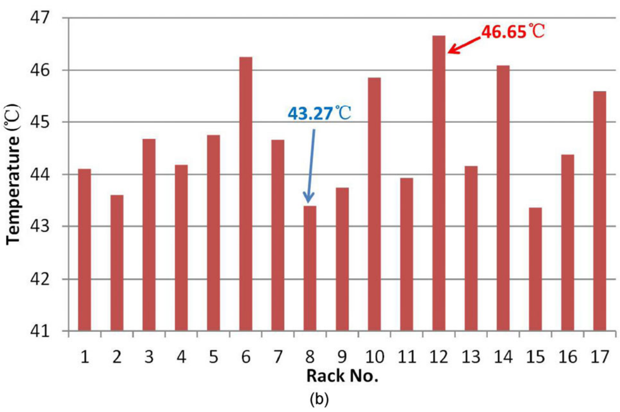

Fig. 26 Hourly averaged temperature inside 17 new racks after retrofitting in 2017: (a) exhaust air of LHP1; (b) intake air of LHP2

testing locations, testing period and server workload are the same as former racks before retrofitting. The hourly averaged room temperature during testing is illustrated by Fig. 27.

It can be clearly seen from Fig. 26 that, after the retrofitting, the air temperature distribution inside cabinets becomes far more uniform. The maximum temperature difference of server intake air reduces from 8.74 °C to 2.57 °C, and that of server exhaust air reduces from 13.06 °C to 3.38 °C. The temperature difference between cabinet exhaust air and room air is within ±1.1 °C. The testing results show a good agreement with initial design object, and testify the effectiveness of such cabinet cooling scheme.

Figure 28 measures the real time temperature of inlet chilled water during the same testing period. Compared with that illustrated by Fig. 19(b), it can be clearly seen that, after retrofitting, the chilled water temperature increases 5–6 °C. The testing result agrees well with the entransy dissipation analysis (5.2 K) in Section 3.3.1. This test shows persuasive and solid proof of the value of entransy theory in data center thermal management.

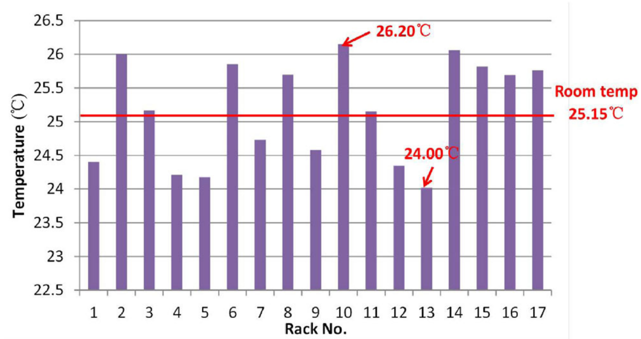

Fig. 27 Hourly averaged temperature of rack exhaust air and data center room after retrofitting in 2017

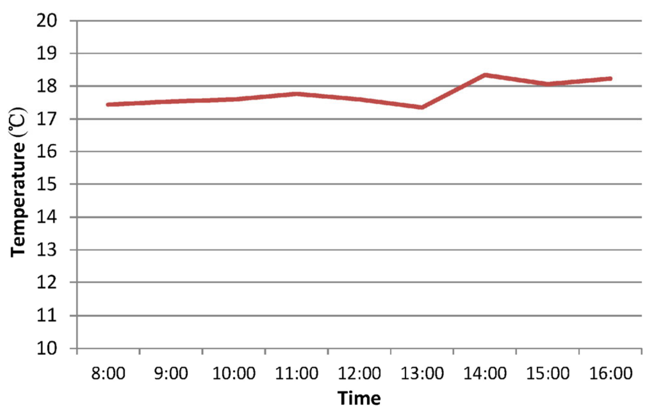

Fig. 28 Real time temperature of chilled water after retrofitting in 2017

4 Conclusion

Based on theoretical derivation, CFD simulation and retrofitting test, the entransy analysis model is built and testified for data center thermal management. Several important points have been concluded as follows:

(1) Air mixing has significant impact on both thermal and energy performance of data centers. The most obvious consequences are more hot spots and more energy cost.

(2) Sealed cold/hot aisles do not eliminate air mixing.

(3) Entransy dissipation analysis can quantify the energy

cost paid for air mixing, by calculating the reduction of chilled water temperature and annual free cooling hours.

(4) Entransy dissipation field can identify the locations where the measures to prevent air mixings will be most effective. It guides thermal managers to work on the right place to optimize data center thermal management.

(5) A new cabinet cooling solution is proposed and testified to eliminate air mixing.

(6) Entransy theory offers a new method to the analysis and optimization of data center thermal management.

Acknowledgements

This study is financially supported by the National Key R&D Program of China (Grant No. 2016YFB0601600).

References

Almoli A, Thompson A, Kapur N, Summers J, Thompson H, Hannah G (2012). Computational fluid dynamic investigation of liquid rack cooling in data centres. *Applied Energy*, 89: 150–155.

Amip JS (2005). Exergy-based analysis and optimization of computer thermal management systems. PhD Thesis, University of California Berkeley, USA.

Carbó A, Oró E, Salom J, Canuto M, Macías M, Guitart J (2016). Experimental and numerical analysis for potential heat reuse in liquid cooled data centres. *Energy Conversion and Management*, 112: 135–145.

Chen Q, Liang XG, Guo ZY (2013). Entransy theory for the optimization of heat transfer—A review and update. *International Journal of Heat and Mass Transfer*, 63: 65–81.

Chen Q, Fu RH, Xu YC (2015). Electrical circuit analogy for heat transfer analysis and optimization in heat exchanger networks. *Applied Energy*, 139: 81–92.

Cheng X, Liang X (2018). Analyses of coupled steady heat transfer processes with entropy generation minimization and entransy theory. *International Journal of Heat and Mass Transfer*, 127: 1092–1098.

Choi J, Kim Y,Sivasubramaniam A, Srebric J, Wang Q, Lee J (2008). A CFD-based tool for studying temperature in rack mounted servers. *IEEE Transactions on Computers*, 57: 1129–1142.

Ebrahimi K, Jones GF, Fleischer AS (2014). A review of data center cooling technology, operating conditions and the corresponding low-grade waste heat recovery opportunities. *Renewable and Sustainable Energy Reviews*, 31: 622–638.

Fulpagare Y, Bhargav A (2015). Advances in data center thermal management. *Renewable and Sustainable Energy Reviews*, 43: 981–996.

Gao T, David M, Geer J, Schmidt R, Sammakia B (2015). Experimental and numerical dynamic investigation of an energy efficient liquid cooled chiller-less data center test facility. *Energy and Buildings*, 91: 83–96.

Garimella SV, Persoons T, Weibel J, Yeh LT (2013). Technological drivers in data centers and telecom systems: Multiscale thermal, electrical, and energy management. *Applied Energy*, 107: 66–80.

Goudarzi N, Talebi S (2018). Heat removal ability for different orientations of single-phase natural circulation loops using the entransy method. *Annals of Nuclear Energy*, 111: 509–522.

Guo Z, Cheng X, Xia Z (2003). Least dissipation principle of heat transport potential capacity and its application in heat conduction optimization. *Chinese Science Bulletin*, 48: 406–410.

Guo ZY, Zhu HY, Liang XG (2007). Entransy—A physical quantity describing heat transfer ability. *International Journal of Heat and Mass Transfer*, 50: 2545–2556.

Guo ZY (2008). New physical quantities in heat. *Journal of Engineering Thermophysics*, 29: 112–114. (in Chinese)

Ham SW, Kim MH, Choi BN, Jeong JW (2015). Simplified server model to simulate data center cooling energy consumption. *Energy and Buildings*, 86: 328–339.

Han Y, Wang D, Zhang C, Zhu Y (2017). The entransy degeneration and entransy loss equations for the generalized irreversible Carnot engine system. *International Journal of Heat and Mass Transfer*, 106: 895–907.

He Z, He Z, Zhang X, Li Z (2016). Study of hot air recirculation and thermal management in data centers by using temperature rise distribution. *Building Simulation*, 9: 541–550.

Herlin MK (2005). Rack cooling effectiveness in data centers and telecom central offices: The rack cooling index (RCI). *ASHRAE Transactions*, 111(2): 725–732.

Hua YC, Zhao T, Guo ZY (2018). Optimization of the one-dimensional transient heat conduction problems using extended entransy analyses. *International Journal of Heat and Mass Transfer*, 116: 166–172.

Kritikos K, Albanakis C, Missirlis D, Vlahostergios Z, Goulas A, Storm P (2010). Investigation of the thermal efficiency of a staggered elliptic-tube heat exchanger for aeroengine applications. *Applied Thermal Engineering*, 30: 134–142.

Liu W, Liu ZC, Jia H, Fan AW, Nakayama A (2011). Entransy expression of the second law of thermodynamics and its application to optimization in heat transfer process. *International Journal of Heat and Mass Transfer*, 54: 3049–3059.

Missirlis D, Yakinthos K, Palikaras A, Katheder K, Goulas A (2005). Experimental and numerical investigation of the flow field through a heat exchanger for aero-engine applications. *International Journal of Heat and Fluid Flow*, 26: 440–458.

Missirlis D, Yakinthos K, Storm P, Goulas A (2007). Modeling pressure drop of inclined flow through a heat exchanger for aero-engine applications. *International Journal of Heat and Fluid Flow*, 28: 512–515.

Nada SA, Elfeky KE, Attia Ali MA, Alshaer WG (2015a). Thermal management of electronic servers under different power conditions. *International Journal of Emerging Trends in Electrical and Electronics*, 11: 145–150.

Nada SA, Rady MA, Elsharnoby M, Said MA (2015b). Numerical investigation of cooling of electronic servers racks at different locations and spacing from the data center cooling unit. *International Journal of Current Engineering and Technology*, 5: 3448–3456.

Nada SA, Elfeky KE (2016). Experimental investigations of thermal managements solutions in data centers buildings for different arrangements of cold aisles containments. *Journal of Building Engineering*, 5: 41–49.

Nada SA, Attia Ali MA, Elfeky KE (2016a). Experimental study of solving thermal heterogeneity problem of data center servers. *Applied Thermal Engineering*, 109: 466–474.

Nada SA, Elfeky KE, Attia Ali MA (2016b). Experimental investigations of air conditioning solutions in high power density data centers using a scaled physical model. *International Journal of Refrigeration*, 63: 87–99.

Nada SA, Said MA, Rady MA (2016c). Numerical investigation and parametric study for thermal and energy management enhancements in data centers' buildings. *Applied Thermal Engineering*, 98: 110–128.

Priyadumkol J, Kittichaikarn C (2014). Application of the combined air-conditioning systems for energy conservation in data center. *Energy and Buildings*, 68: 580–586.

Rambo J, Joshi Y (2007). Modeling of data center airflow and heat transfer: State of the art and future trends. *Distributed and Parallel Databases*, 21: 193–225.

Sharma RK, Bash CE, Patel CD (2002). Dimensionless parameters for evaluation of thermal design and performance of large scale data centers. In: Proceedings of 8th AIAA/ASME Joint Thermophysics and Heat Transfer Conference, St. Louis, MO, USA, pp. 3091–3101.

Shrivastava SK, VanGilder JW, Sammakia BG (2009). Prediction of cold aisle end airflow boundary conditions using regression modeling. *IEEE Transactions on Components and Packaging Technologies*, 30: 866–874.

Song Z (2016). Numerical cooling performance evaluation of fan-assisted perforations in a raised-floor data center. *International Journal of Heat and Mass Transfer*, 95: 833–842.

Tian H, He Z, Li Z (2015). A combined cooling solution for high heat density data centers using multi-stage heat pipe loops. *Energy and Buildings*, 94: 177–188.

Van Gilder JW, Pardey Z, Healey CM, Zhang X (2013). A compact server model for transient data center simulations. *ASHRAE Transactions*, 119(2): 358–370.

Wang C, Zhu Y (2017). Optimization of double-stage latent heat storage unit in whole cycle with entransy analysis. *International Journal of Heat and Mass Transfer*, 114: 1013–1024.

Wang S, Jian G, Wang J, Sun L, Wen J (2018a). Application of entransy-dissipation-based thermal resistance for performance optimization of spiral-wound heat exchanger. *International Journal of Heat and Mass Transfer*, 116: 743–750.

Wang XJ, He YL, Wang ZD, Tao WQ (2018b). Microscopic expression of entransy in ideal gas system for diatomic molecules. *International Journal of Heat and Mass Transfer*, 127: 1347–1350.

Wang XY, Zhao XL, Fu L (2018c). Entransy analysis of secondary network flow distribution in absorption heat exchanger. *Energy*, 147: 428–439.

Wei H, Du X, Yang L, Yang Y (2017). Entransy dissipation based optimization of a large-scale dry cooling system. Applied Thermal Engineering, 125: 254–265.

Wei S, Chen L, Xie Z (2018). Constructal heat conduction optimization: Progresses with entransy dissipation rate minimization. *Thermal Science and Engineering Progress*, 7: 155–163.

Wen J, Gu X, Wang M, Liu Y, Wang S (2018). Multi-parameter optimization of shell-and-tube heat exchanger with helical baffles based on entransy theory. *Applied Thermal Engineering*, 130: 804–813.

Xu M (2011). The thermodynamic basis of entransy and entransy dissipation. *Energy*, 36: 4272–4277.

Yakinthos K, Missirlis D, Palikaras A, Storm P, Simon B, Goulas A (2007). Optimization of the design of recuperative heat exchangers in the exhaust nozzle of an aero engine. *Applied Mathematical Modelling*, 31: 2524–2541.

Zhang H, Shao S, Xu H, Zou H, Tian C (2014). Free cooling of data centers: A review. *Renewable and Sustainable Energy Reviews*, 35: 171–182.

Zhou JH, Yang CX (2008). Design and simulation of the CPU fan and heat sinks. *IEEE Transactions on Components and Packaging Technologies*, 31: 890–903.

Zhou JH, Yang CX (2010). Parametric design and numerical simulation of the axial-flow fan for electronic devices. *IEEE Transactions on Component Packaging Technology*, 33: 287–298.

Zhou R, Wang Z, Bash CE, McReynolds A (2012). Data center cooling management and analysis—A model based approach. In: Proceedings of the 28th Annual IEEE Semiconductor Thermal Measurement and Management Symposium (SEMI-THERM), San Jose, CA, USA, pp. 98–103.

Zhou B, Cheng X, Wang W, Liang X (2015). Entransy analyses of thermal processes with variable thermophysical properties. *International Journal of Heat and Mass Transfer*, 90: 1244–1254.